INT. J. NUM. METH. HEAT FLUID FLOW, VOL. 4, 3–29 (1994)

NUMERICAL SIMULATION OF COMPRESSIBLE FLOW INDUCED BY A HEAT AND MASS SOURCE IN A PARTIALLY-OPEN CAVITY

L. ALLANÇON, B. PORTERIE, R. SAUREL AND J. C. LORAUD

IUSTI/SETT—Equipe Ecoulements Diphasiques et Réactifs—URA CNRS 1168, Université de Provence—Centre de Saint-Jérôme, 13397 Marseille Cedex 20, France

ABSTRACT

A numerical analysis is given for the prediction of unsteady, two-dimensional fluid flow induced by a heat and mass source in an initially closed cavity which is vented when the internal overpressure reaches a certain level. A modified ICE technique is used for solving the Navier–Stokes equations governing a compressible flow at a low Mach number and high temperature. Particular attention is focused on the treatment of the boundary conditions on the vent surface. This has been treated by an original procedure using the resolution of a Riemann problem. The configuration investigated may be viewed as a test problem which allows simulation of the ventilation and cooling of such cavities. The injection of hot gases is found to play a key role on the temperature field in the enclosure, whereas the vent seems to produce a distortion of the dynamic flow-field only. When the injection of hot gases is stopped, the enclosure heat transfer is strongly influenced by the vent. A comparison with the results obtained when the radiative heat transfer between the walls of the enclosure is considered, indicate that radiation dominates the heat transfer in the enclosure and alters the flow patterns significantly.

KEY WORDS Compressible flow Ventilation Heat transfer

NOMENCLATURE

a	speed of sound
A_l	location ratio ($A_l = L_1/L$) (see *Figure 1*)
A_0	opening ratio ($A_0 = dSe/L$) (see *Figure 1*)
C_v	specific heat of fluid at constant volume
C_p	specific heat of fluid at constant pressure
e	specific internal energy of the gas
g_y	gravitational acceleration
H	enclosure height
$J(k, rk)$	radiosity of wall k at position rk
k	thermal conductivity of the gas
L	enclosure width
$\dot{m}$	mass flow-rate
$\dot{m}_{max}$	maximal rate of mass injected
$\dot{m}_s$	mass flow-rate per unit area
M_{total}	total mass injected
P	pressure of the gas
P_{tank}	pressure of the infinite tank
T	temperature of the gas
T_{ci0}	initial temperature of the injected gas
T_{cif}	final temperature of the injected gas
$T_{rad}(k, rk)$	temperature of wall k at position rk
T_{tank}	temperature of the infinite tank
u, t	components of the velocity of the gas in the x and y directions
x, y	coordinates along the horizontal direction and vertical direction

Greek symbols

β	volume expansion coefficient at constant pressure
γ	ratio of the specific heats
μ	viscosity of the gas
$\varepsilon(k)$	emissivity of wall k
ρ	density of the gas
$\rho(k)$	reflectivity of wall k
σ	Stefan–Boltzmann constant
Φ_{rad}	net radiant heat flux of wall
$\phi_{rad}(k, rk)$	net density of radiant heat flux of wall k at position rk

0961–5539/94/010003–27$2.00

Received December 1992
Revised June 1993

Subscripts

0	reference state
k	wall k
l	left state in the Riemann problem
r	right state in the Riemann problem
rk	position on wall k

INTRODUCTION

The transport of heat and mass by buoyancy-induced convective motion is a mechanism which finds relevance in many physical systems (building or nuclear reactor insulation, double-pane windows, solar collectors, enclosed fires, etc.). It is for this reason that natural-convection heat transfer in cavities has received considerable attention for several years. A large number of numerical or experimental studies have been devoted to natural convection in differentially-heated cavities when the hot and the cold walls are vertical[1–3]. In the last decade, this idealized problem has been extensively studied in various contexts; inclined enclosures containing internal heat sources[4,5] and radiation combined with other modes of heat transfer in a multidimensional cavity[6,7]. Recent studies have focused on the analysis of natural convection in open cavities because of its important role in solar thermal central receiver systems as well as other engineering systems (electronic equipment, etc.), to minimize and predict heat losses. Penot[8], Le Quere *et al.*[9] and Chan and Tien[10] have examined laminar natural convection heat transfer in two-dimensional rectangular open cavities using the Boussinesq approximation and the finite difference method. Miyamoto *et al.*[11] have studied the effects of an aperture and cavity orientation, with respect to the direction of gravity, on steady laminar natural convective heat transfer in the cavity. Humphrey and To[12] have analyzed, theoretically, turbulent free convection heat transfer in a square open cavity. Experimental studies have been performed by Humphrey *et al.*[13], Sernas and Kyriakides[14], Hess and Henze[15], Chen *et al.*[16] and Chan and Tien[17]. Other problems involving natural convection in open cavities have been studied by Doria[18] in predicting fire spread in a room, and we can quote the work of Sefcik, Webb and Heaton[19], as an example, where the buoyancy-driven flow and heat transfer are restricted by vents in the top and bottom walls of the enclosure. Yang[20] and Ostrach[21] presented surveys of experimental and numerical studies prior to 1988. Nevertheless, a large number of these studies have been made with vertical walls heated at a uniform temperature and within the approximation which takes into account the density variation in the buoyancy term, but neglects it in the inertial terms of the equations of motion. The conditions under which this traditional Boussinesq approximation applies to a given Newtonian liquid or gas have been known since the work of Gray and Giorgini[22]. This assumption is least correct for high-Grashoff number problems, when the temperature differences in the enclosure are large. This is the reason why, in the study of flows with large temperature gradients (theoretically superior to 10% in the case of air), the conditions for the validity of the Boussinesq approximation are not satisfied, and it is necessary to solve a compressible flow at a low Mach number and high temperature. The difficulty with this kind of problem is manifest in the large discrepancy which exists between the flow and the velocity of sound, which requires a specific numerical treatment of the equations because of their stiffness, as discussed by Fernandez and Guillard[23] for the case of low Mach number reactive flows.

In the last decade, understanding the phenomena of coupled heat and mass transfer in cavities subject to high temperature has found important applications in the safety assessment of nuclear reactors, buildings, etc. The knowledge of the behaviour of concrete under fire (pressure, temperature) is important to achieve more effective methods of detection and control. In recent years, there has been considerable research interest in CFD regarding enclosed high-temperature or reactive flows. The present work is related to these topics.

Specifically, a numerical study of the flow induced by an internal heat and mass source in an initially closed cavity has been developed. The large increase of temperature and pressure being

generated triggers the opening of a vent in the ceiling of the cavity, simulating the ventilation and cooling of the enclosure. The Boussinesq approximation cannot be used in this study and because of the injection of hot gases in a closed cavity and the large temperature differences and also due to the necessity to compute the pressure build-up in the cavity. Therefore we must solve a low-Mach number, high-temperature compressible flow problem. A modified ICE method (Implicit Continuous-fluid Eulerian)[24] is proposed for solving the 2D unsteady Navier–Stokes equations. Particular attention is needed for the treatment of the boundary conditions after the opening of the vent; to this purpose, we refer to the resolution of a Riemann problem. This original procedure allows accurate treatment of an outgoing flow and a possible incoming one. In this paper the response of the enclosed fluid to a heat and mass source is studied, including the effects of the opening of the enclosure and the effects of the radiant heat transfer upon the flow patterns.

ANALYSIS

Physical model

The model used for the study is as shown in *Figure 1*. A two-dimensional rectangular enclosure is surrounded by walls, supposed adiabatic. As initial conditions, we assume that the enclosed air and walls are at the ambient temperature and the air is stagnant. At time $t = 0$, a specified heat and mass source is placed somewhere on the floor of the cavity. Hot gases, whose final temperature is about 1500 K, are produced by the source until time t_3. The enclosed air mixes with the hot source gases and moves convectively due to the gradients of temperature. The temperature and the pressure of the enclosed fluid increase until an overpressure equal to 500 mbar develops, when the surface *dSe*, in the ceiling of the cavity, opens. The hot gases can flow out of the cavity to the exterior, settling to atmospheric pressure and ambient temperature.

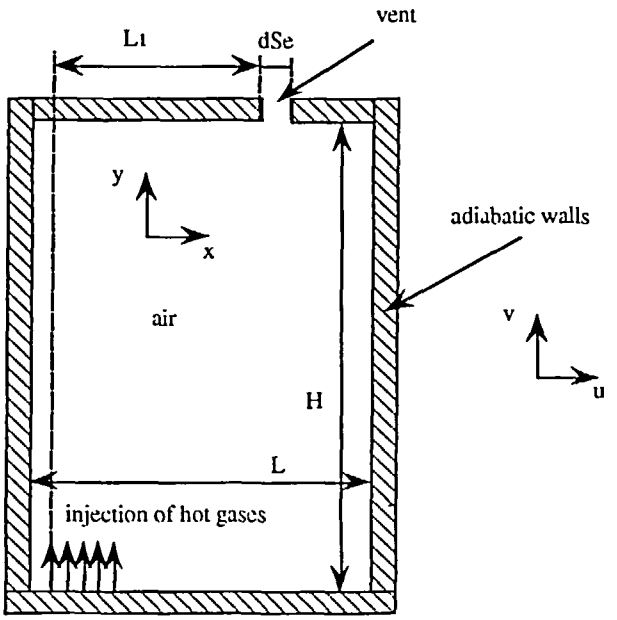

Figure 1

Table 1 Injection model

For the mass flow-rate $\dot{m}$:		For the temperature T:
$0 \leqslant t < t_1$	$\dot{m} = \dot{m}_{max}\dfrac{t}{t_1}$	$T = T_{ci0} + (T_{cif} - T_{ci0})\dfrac{t}{t_1}$
$t_1 \leqslant t < t_2$	$\dot{m} = \dot{m}_{max}$	$T = T_{cif}$
$t_2 \leqslant t < t_3$	$\dot{m} = \dot{m}_{max}\dfrac{t - t_3}{t_2 - t_3}$	$T = T_{cif}$
$t_3 \leqslant t$	$\dot{m} = 0$	$\dfrac{\partial T}{\partial y} = 0$

with:

$$\dot{m}_{max} = \frac{M_{total}}{\dfrac{t_2}{2} - \dfrac{t_1}{2} + \dfrac{t_3}{2}}$$

The basic assumptions made in this analysis are as follows:

(i) the fluid motion and heat transfer processes are two-dimensional and unsteady;
(ii) the fluid flow is laminar, and the fluid physical and transport properties are constant;
(iii) viscous dissipation terms are neglected in the energy equation;
(iv) the heat and mass source produces hot gases whose temperature and mass flow rate vary as a function of time, conveniently taken, so as to avoid large initial gradients of temperature and mass, which can generate discontinuities at the boundary during the initial time steps. After these stages, flow rate and temperature settle to constant values.

The model for the injection is reported in *Table 1* where T_{ci0} and T_{cif} are, respectively, the initial and final temperature of the gas injected in the cavity, $\dot{m}_{max}$ is the maximal rate of mass injected, M_{total} is the total mass injected in the cavity;

(v) this injection of gas is assumed to take place normal to the cavity floor, so that $u = 0$;
(vi) the flow is ejected perpendicularly through the cavity ceiling to an infinite tank modelling the atmosphere with constant conditions, thus: $P_{tank} = P_{atm}$ and $T_{tank} = 300$ K and $u = v = 0$.
(vii) for this analysis, the radiative heat transfer between the walls of the cavity could be considered. In this case, the walls are treated as grey diffuse surfaces and the vent as a black surface[25]. The confined fluid is assumed to be radiatively non-participating (similar to the hot gases injected).

Because of the size of most enclosures where fires develop, the validity of the assumptions of two-dimensional heat transfer processes and laminar fluid flow can be questioned. Three-dimensional effects will be present and fully developed fires are highly turbulent. However, this paper does not pretend to study an enclosed fire without taking into account a reactive model. Moreover, considerable insight into the flow phenomena and heat transfer of the problem can be gained without initially introducing the very complex turbulent three-dimensional motion. The assumption of constant transport physical properties is a numerical convenience and is frequently used in generalized studies in order to decrease the number of independent parameters. The third assumption is justifiable in comparison with conduction and convection heat dissipation. The model for the injection of gases can, for example, be adopted to simulate the thermal degradation of fuel surface. The assumption of grey diffuse surfaces is often used in most studies about radiative heat transfer. In addition, Toor and Viskanta[26] have shown that, for most enclosures, the assumption of grey diffuse walls is a reasonable approximation to reality.

In convective processes, the radiative heat transfer may affect the temperature field and hence the flow field, directly through absorption and emission processes within the fluid. This effect may be small, for example if the fluid is dry air. Radiation may also have an effect on the flow field indirectly through the temperature distribution on solid boundaries. Also, emission of radiation by the boundaries as well as radiative interaction between them have an important bearing on the boundary temperature.

Mathematical model

Governing equations

The governing equations relating to the gas are the well-known, compressible Navier–Stokes equations. For an unsteady two-dimensional real fluid, the continuity, momentum and energy equations are written in cartesian coordinates as:

Continuity equation

$$\frac{\partial \rho}{\partial t} + \frac{\partial \rho u}{\partial x} + \frac{\partial \rho v}{\partial y} = 0 \tag{1}$$

Momentum equations

$$\rho\left(\frac{\partial u}{\partial t} + u\frac{\partial u}{\partial x} + v\frac{\partial u}{\partial y}\right) = -\frac{\partial P}{\partial x} + \mu\left(\frac{4}{3}\frac{\partial^2 u}{\partial x^2} + \frac{\partial^2 u}{\partial y^2} + \frac{1}{3}\frac{\partial^2 v}{\partial x \partial y}\right) \tag{2}$$

$$\rho\left(\frac{\partial v}{\partial t} + u\frac{\partial v}{\partial x} + v\frac{\partial v}{\partial y}\right) = \rho g_y - \frac{\partial P}{\partial y} + \mu\left(\frac{4}{3}\frac{\partial^2 v}{\partial y^2} + \frac{\partial^2 v}{\partial x^2} + \frac{1}{3}\frac{\partial^2 u}{\partial x \partial y}\right) \tag{3}$$

Internal energy equation

$$\rho\left(\frac{\partial e}{\partial t} + u\frac{\partial e}{\partial x} + v\frac{\partial e}{\partial y}\right) = -P\left(\frac{\partial u}{\partial x} + \frac{\partial v}{\partial y}\right) + k\left(\frac{\partial^2 T}{\partial x^2} + \frac{\partial^2 T}{\partial y^2}\right) \tag{4}$$

Here we have assumed that the viscosity μ is constant and that the second coefficient of viscosity λ obeys to the Stokes equation: $3\lambda + 2\mu = 0$. The specific heat at constant volume C_v and the thermal conductivity k are constant and are related to the Prandtl number and viscosity by the relation:

$$\mathrm{Pr} = \mu\gamma C_v/k$$

We assume also that the gas obeys the ideal gas equation of state:

$$P = (\gamma - 1)\rho e$$

with

$$e = C_v T$$

and

$$\gamma = C_p/C_v$$

If the radiative heat transfer is considered, the above equations are coupled with the following energy balance equation at the adiabatic walls[7]:

$$\Phi_{\mathrm{rad}} = k\frac{\partial T}{\partial n} \tag{5}$$

where n represents the coordinate normal to the wall.

Equation (5) is a boundary condition which couples the radiative, convective and conductive

heat transfer in the enclosure. Any change in the wall surface temperature simultaneously affects the convection to the wall and the net radiant heat flux at the wall. The density of radiative flux along wall k at the position rk is given by:

$$\phi_{\text{rad}}(k, rk) = \frac{\varepsilon(k)}{\rho(k)} [\sigma T^4_{\text{rad}}(k, rk) - J(k, rk)] \tag{6}$$

where $\varepsilon(k)$ and $\rho(k)$ are the emissivity and reflectivity respectively of wall k and the radiosity $J(k, rk)$ for plane walls is given by[26]:

$$J(k, rk) = \varepsilon(k)\sigma T^4_{\text{rad}}(k, rk) + (1 - \varepsilon(k)) \sum_{l=1}^{N} \int_{A_l} J(l, rl)\, \mathrm{d}F_{dA_k - dA_l} \tag{7}$$

$\mathrm{d}F_{dA_k dA_l}$ is a function of the configuration. The radiative model and computational resolution is given in more detail in Allançon *et al.*[71].

NUMERICAL METHOD

Choice of the method

In numerical studies on convection in cavities, the problem is usually simplified to a cavity model with isothermal hot and cold boundaries; the solution is based upon the Boussinesq approximation, which assumes the fluid to be incompressible but expansive; then, the gas density is only a linear function of the temperature. We can write the relation which replaces the equation of state:

$$\frac{\rho}{\rho_0} = \frac{1}{1 + \beta(T - T_0)} \cong 1 - \beta(T - T_0)$$

where T and ρ are, respectively, the temperature and the density of the gas, and the subscript 0 denotes the reference state. β is the thermal expansion coefficient defined by:

$$\beta = -\frac{1}{\rho_0}\left(\frac{\partial \rho}{\partial T}\right)_P$$

However, in our analysis, we cannot use this approximation of an incompressible fluid, because some mass is injected in an initially closed cavity. Therefore, a physical incompatibility appears between the injection of mass and the motion of an incompressible fluid surrounded by a closed cavity, even in the case of low velocities of injection. Moreover, the knowledge of pressure values is of capital importance, because the cavity opens to the exterior at an overpressure equal to 0.5 bar; and the computation of the pressure with the Boussinesq approximation would be erroneous due to the assumption of incompressibility. In addition to that, even if the real limits of validity of the Boussinesq approximation are not yet definitely known, theoretical limits have been proposed by Gray and Giorgini[22] in the cases of air and water, respectively:

$$\Delta T/T_0 \leqslant 0.10 \quad \text{and} \quad \Delta T/T_0 \leqslant 0.0043 \quad (\text{when } T_0 = 288 \text{ K})$$

where ΔT is the difference between the hot temperature and the temperature of the reference state—the Boussinesq approximation becomes invalid at high values of the temperature gradient. Therefore, to solve our problem, we had to consider the full compressible Navier–Stokes equations. Numerical methods for solving these equations are numerous. The most popular finite-difference methods are the Beam and Warming scheme[27] and the MacCormack explicit or implicit schemes[28,29]. More recently, finite volume schemes, used to solve hyperbolic systems of partial differential equations, have been successfully extended to the Navier–Stokes equations (Van Leet[30] etc.).

However, the explicit technique is very attractive because of the simplicity of use and the small number of calculations during a time step, but this kind of scheme is limited by the value of the time step due to the stability conditions. So, at first view, such a technique would not have been interesting for our analysis owing to the time for simulation (about 30 sec), and the required time step, of the order of 10^{-6} sec. The choice between explicit and implicit schemes is a controversial decision. Implicit schemes for the convective derivatives involve, in the worst cases, gigantic matrix equations, and in the best cases, the inversion of a tridiagonal matrix. Therefore, their operation counts and speeds are appreciably worse than the performance obtained using the corresponding explicit schemes. The advantage of implicit schemes, which in some problems outweighs the dual disadvantages of program complexity and operation count per time step, is the ability to accept much larger finite difference time steps without exciting numerical modes of instability. The choice between explicit and implicit differencing lies in the physics (or in the mathematics) of the specific problem being solved. When the physical phenomenon of interest varies appreciably on a time scale τ, no calculation with $\Delta t \gg \tau$, can reasonably be claimed to reproduce the phenomenon accurately.

Moreover, our study is devoted to an unsteady compressible flow at low Mach number, and implicit methods lose a lot of their interest for this kind of problem due to the treatment of the boundary points. This treatment needs a time step which cannot be really larger than the explicit one, when there are subsonic boundaries and large source terms[31]. Also, the results obtained for subsonic compressible flows with a classical or current implicit or explicit method (MacCormack, Beam and Warming) are not accurate when the ratio between the maximum and the minimum eigenvalues of the Jacobian matrix of the system is too large. In our case, the values of the gas velocity v and the sound speed a are respectively about 1 m/s and 1000 m/s near the injection points of the hot gases. Therefore, the ratio $(v + a)/v$ is about 1000, and it is really too large (problem of a poorly-conditioned matrix).

It is for all those reasons that we have chosen a modified ICE technique developed by Harlow and Amsden[24] which avoids the disadvantages of classical explicit and implicit schemes, to solve the compressible Navier–Stokes equations.

ICE technique

This method is useful for the numerical solution of time-dependent problems in multidimensional fluid dynamics for all Mach numbers from zero (incompressible limit) to infinity (hypersonic limit). In this technique, the system of PDE is solved under the form written in (1), (2), (3) and (4). The finite difference mesh used for solving the above equations consists of rectangular cells of width Δx and height Δy. A fragment of the finite difference mesh is shown in *Figure 2*, which illustrates the centering of the field variables relative to a typical cell. The index i counts cell centers from left to right, while the cells in the y-direction are labelled with the index j from bottom to top. Quantities defined at cell edges are labelled with indices $i^{\pm 1/2}$ or $j^{\pm 1/2}$. The dependent variables are located within a cell as shown above: u, the horizontal component of the velocity, at the middle of the vertical sides; v, the vertical component of the velocity, at the middle of the horizontal sides; and all other variables are evaluated at the cell center. The fluid region is surrounded by a single layer of fictitious cells, *Figure 3*.

The continuity equation is differenced in terms of cell-centered gradients of mass fluxes through cell walls. These fluxes consist of two components; a spatially centered term and a donor cell (or upwind) term. The momentum equations are similarly differenced, although the convective terms are not written in terms of momentum fluxes, but as edge-centered fluxes of a velocity gradient (see the appendix). The difference equation for the internal energy is similar to those for the momenta. The equation to be solved simultaneously with the transport equations is:

$$P_{i,j} - F(\rho_{i,j}, e_{i,j}) = 0$$

where F is the equation of state.

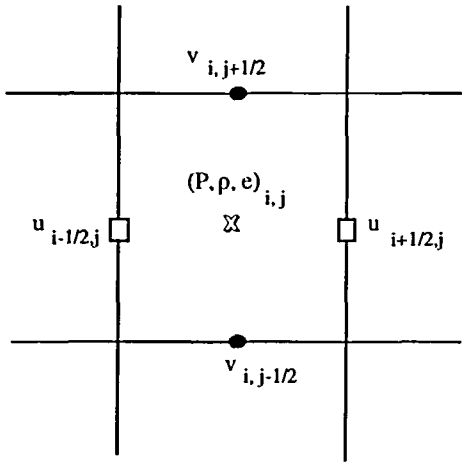

Figure 2 Typical finite difference mesh

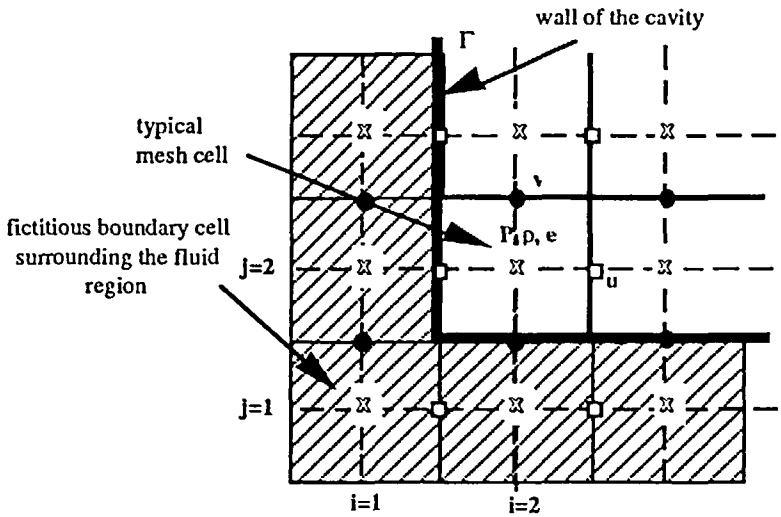

Figure 3 Cell distribution of variables

An iterative procedure for the pressure is used until the following convergence criterion is satisfied:

$$|\delta P^{(v)}| \leqslant \varepsilon \bar{P}_{i,j}^{(v+1)}, \quad \varepsilon \geqslant 0$$

where ε is a parameter of convergence tolerance, and the superscript v denotes the iterative count, while $\bar{P}$ is the estimate of the pressure at the advanced time.

Treatment of the boundary conditions

Boundary conditions are easily imposed by setting appropriate values of the dependent variables in the fictitious cells surrounding the mesh. One must treat three kinds of boundary

conditions:

- the walls of the cavity as rigid boundaries;
- the injection of hot gases from the floor of the cavity;
- the ejection of some gases out of the cavity to an infinite tank through an opening somewhere on the ceiling.

For a rigid boundary, owing to adiabatic boundary condition, the normal gradient of temperature (or energy) is zero; solid walls and zero slip at the walls imposes that the normal and the tangential velocity components, respectively be equal to zero. The variable ρ is treated in the same way as T (or e). If the radiative heat transfer is considered the boundary condition for the temperature is determined by the energy balance equation written previously. Once the radiative fluxes have been determined, the temperatures of the boundaries can be calculated from equations (5)–(7), which couple the radiation and convection heat transfers[7].

For the injection of hot gases through the floor, a specified temperature source at some location on the floor is imposed, of an intensity varying as a function of time, and likewise for the mass flowrate. Moreover, we have assumed that the injection of hot gases is normal to the floor, so, $u = 0$.

The v-component of the velocity, the density and the pressure are deduced from the equations:

$$\rho_1 v_1 = \dot{m}_s$$

with $\dot{m}_s$ the mass flow-rate of injected gases per unit area.

$$\mathrm{P} = \rho \mathrm{RT}$$

$$P_1 + \rho_1 v_1^2 = P_2 + \rho_2 v_2^2$$

where the subscripts 1 and 2 denote, respectively, the injection points and the immediately neighbouring interior points.

It would appear that, for the outflow boundary conditions on the ceiling vent, the problem might be treated in the same way as the inflow conditions, but the problem is complicated by the fact that we do not know the temperature and the mass flow rate of the ejected gases. Moreover, the problem is rendered difficult because the ejected flow is subsonic. In this case, the boundary conditions must take account of the exterior conditions, whereas for the case of supersonic exit, the variables can be extrapolated. In addition to that, the model to be used should be able to deal both with outcoming flow from the cavity, and possible incoming cool flow into the cavity from the exterior. To solve this problem one can use the method of characteristics; but the disadvantage of this method is the iterative building of the characteristic grid which needs a double interpolation procedure. Moreover, according to the sign of the flow velocity, one has to take a different characteristic scheme. In view of all these, we have chosen to consider another numerical method, and to treat the problem of the exit condition as the solution of a Riemann problem.

Solution of a Riemann problem

The solution of a Riemann problem[32] avoids for the present study the disadvantages of the characteristics method. Thus, there are no interpolation difficulties, and the method takes direct account of inflow and outflow by referring to the immediately neighbouring points. One assumes that during a time step equal to the CFL time step, the flux is constant. This flux is taken constant during the entire time step chosen for the overall numerical solution. In the exit section, the equations governing the flow are given by:

$$\frac{\partial}{\partial t}[V] + \frac{\partial}{\partial y}[f(V)] = h(V, y) \tag{8}$$

where

$$V = \begin{bmatrix} \rho \\ \rho v \\ \rho e \end{bmatrix} \quad \text{and} \quad f(v) = \begin{bmatrix} \rho v \\ \rho v^2 + P \\ v(\rho e + P) \end{bmatrix} \quad \text{and} \quad h(v, y) = \begin{bmatrix} 0 \\ \rho g_y \\ 0 \end{bmatrix}$$

The first step is to find a solution to a simpler set of the original equations. This simpler set is that of the homogeneous equations, and is given by:

$$\frac{\partial}{\partial t}[V] + \frac{\partial}{\partial y}[f(V)] = 0 \tag{9}$$

Once the solution V, for this simpler set of equations is obtained, it can be corrected for the missing inhomogeneous part $h(V, y)$. This correction is done using the operator splitting technique. To start with, however, the analysis will be restricted to the homogeneous equations (9).

As it is well known, a Riemann problem is characterized by initial values which are a left state $Sl(\rho_l, a_l, v_l)$ and a right state $Sr(\rho_r, a_r, v_r)$ with the respective distances y_j and y_{j+1} at time t_k, where the density ρ, the sound velocity a and the component of the gas velocity v are known. An initial discontinuity breaks into left- and right-running waves, which are separated by a contact surface. The state behind the left wave on the left side of the contact surface is defined by $Sl(\rho_l^*, a_l^*, v_l^*)$, and in a similar way, the state behind the right wave on the right side of the contact surface is $Sr(\rho_r^*, a_r^*, v_r^*)$, *Figure 4*. Because of the physical conditions and assumptions of our study, we are certain that we cannot have fully-developed shock waves, and therefore we may consider the case of an elemental wave, which can be either a left-running wave or a right-running wave. The states $Sl(\rho_l, a_l, v_l)$ and $Sr(\rho_r, a_r, v_r)$ ahead of a left or right moving rarefaction wave are known. The sound speed, density, and flow velocity behind a left- or right-moving expansion wave are:

$$a_l^* = a_l\left[\frac{P^*}{P_l}\right]^{(\gamma-1)/2\gamma} \qquad a_r^* = a_r\left[\frac{P^*}{P_r}\right]^{(\gamma-1)/2\gamma} \tag{10}$$

$$\rho_l^* = \rho_l\left[\frac{P^*}{P_l}\right]^{1/\gamma} \qquad \rho_r^* = \rho_r\left[\frac{P^*}{P_r}\right]^{1/\gamma} \tag{11}$$

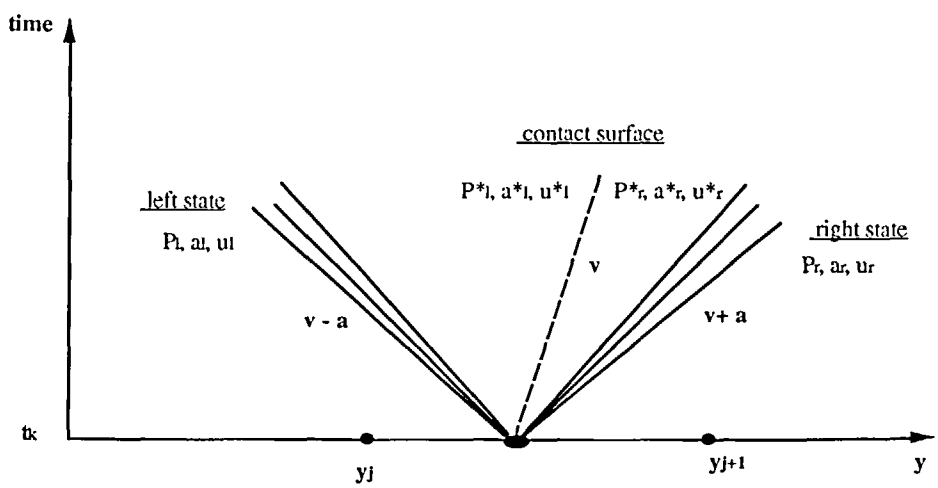

Figure 4 Definition sketch for the Reimann problem

$$v_l^* = v_l + \frac{2}{\gamma - 1}(a_l - a_l^*) \qquad v_r^* = v_r - \frac{2}{\gamma - 1}(a_r - a_r^*) \tag{12}$$

Equations (10) to (12) are the basic expressions needed for determining the solution for a Riemann problem. We can combine relations (10) to (12) to eliminate the common flow velocity $v^* = v_l^* = v_r^*$ on each side of the contact surface, and obtain the value of P^*. This can be done here because we know that the wave model is only composed of simple waves and that equations (10) to (12) are exact for this model. Hence, the guess of P^* is given by:

$$P^* = \left[\frac{a_l + a_r + \dfrac{\gamma - 1}{2}(v_l - v_r)}{\dfrac{a_l}{P_l^{(\gamma-1)/2\gamma}} + \dfrac{a_r}{P_r^{(\gamma-1)/2}}} \right]^{2\gamma/(\gamma-1)} \tag{13}$$

The value of P^* allows computation of the other parameters from the isentropic relations (7) to (9):

$$a_l^*,\ a_r^*,\ v_l^*,\ v_r^*,\ T_l^*,\ T_r^*$$

The Riemann problem resolution is virtually finished. However, to obtain the solution of the complete partial differential equations (8), governing the one-dimensional unsteady motion of a gas in the opening of the cavity, we have to take account of the right-hand side of equation (8). Let then the solution of the homogeneous equations, which is the solution of the Riemann problem, be denoted by $\tilde{V}$. As soon as this Riemann solution is known, the second step is to solve the set of time-split equations given by:

$$\frac{d}{dt}[V] = h(\tilde{V}, y)$$

with:

$$h(\tilde{V}, y) = \begin{bmatrix} h_1 \\ h_2 \\ h_3 \end{bmatrix} = \begin{bmatrix} 0 \\ \tilde{\rho} g_y \\ 0 \end{bmatrix}$$

where h_1, h_2, h_3 are the functions corresponding to the source terms of the equations. In order to obtain the inhomogeneous terms, these simple ordinary differential equations are to be solved using the Cauchy–Euler time-integration method.

RESULTS AND DISCUSSION

To determine a suitable grid size, the computed profiles of velocity and temperature were compared for a number of grid sizes. A uniform grid size was used. After several tries and comparisons of the solution between grid sizes, a final grid size of $22 * 22$ grid points was chosen for this study because it was found to be satisfactory in terms of both accuracy and computing economy. Conservation of mass, momentum and energy was found to be satisfied. Typical computing times on an IBM 3090 for the $22 * 22$ grid chosen and the time step equal to 2.5×10^{-4} sec were of the order of 1.3×10^{-4} sec CPU/point/iteration.

The results are presented in two sections. The first section deals with the thermal heat transfer and dynamic field in a rectangular enclosure due to the injection of hot gases. This section highlights that the heat and mass source and radiative heat transfer in the enclosure dominate this kind of flow. This is evident when comparing the results obtained in three cases: injection of hot gases, injection of hot gases coupled with radiation and natural convection. The second

section concerned a parametric study related to three essential factors: the location of the injection of hot gases, the effects of the opening ratio A_0, the influence of the location of the vent with respect to the injection (location ratio A_l).

General study: heat transfer and dynamic fluid flow

In this first section, the enclosure size is $1\,\text{m} * 2\,\text{m}$. The initial temperature imposed in the cavity is $T_0 = 300$ K, and the initial pressure is equal to 10^5 Pa. The parameter values retained for this simulation are:

$$T_{cif} = 1500\ \text{K}, \quad T_{ci0} = 300\ \text{K}, \quad M_{\text{total}} = 2.5\ \text{kg}$$
$$t_1 = 2\ \text{s}, \quad t_2 = 18\ \text{s}, \quad t_3 = 20\ \text{s}$$
$$\gamma = 1.4, \quad \text{Pr} = 0.7$$
$$t_{\text{final}} = 30\ \text{s}$$

The final temperature T_{cif} of the hot gases is reached at $t_1 = 2$ sec, and the injection of hot gases is stopped at $t_3 = 20$ sec. The thermophysical properties are taken at the reference temperature (T_0).

Forced convection

Figures 5, 6, 7 represent, respectively, the evolutions of velocity, density and temperature at nine different times: $t = 1, 2, 5, 10, 15, 18, 20, 25, 30$ sec. These times have been chosen as best to illustrate the evolution of the flow. For a complete understanding of the phenomena, one should consider the velocity field, the density field, and the corresponding temperature field.

Figure 5 shows the velocity field. At $t = 1$ sec, the injection of hot gases sets the fluid in motion, but essentially is limited to the injection area. A low compression zone is also developing in front of the hot gases: the density is about $1.19\ \text{kg/m}^3$ (see *Figure 6*). In *Figure 7*, we can see the development of the corresponding isotherm lines at the bottom of the cavity, due to the heat transferred by the hot gases injected into the enclosed fluid. As time progresses, isotherms develop quickly to the top of the cavity. This phenomenon is due to the injection of hot gases, which mainly governs the temperature field from $t = 2$ sec. At $t = 2$ sec, the overpressure reaches 500 mbar and triggers the opening of the cavity, when the fluid starts to flow out of the cavity, with a maximum velocity about 7 m/s (*Figure 5*). Because the injection of hot gases and the vent are not in the same positions respectively in the floor and at the top of the cavity, the flow is bent and eddies appear near the main flow, which compresses them (from $t = 5$ sec to $t = 20$ sec).

In *Figure 6*, from $t = 2$ sec, when the cavity opens, isolines of lighter fluid appear (the density varies from $0.4\ \text{kg/m}^3$ to $1.10\ \text{kg/m}^3$), which correspond to the hottest fluid whereas the fluid at high density stays in the right corner at the bottom of the cavity. This part of the cavity corresponds to the small eddy which is the last to be subjected to the heat flux (from $t = 5$ sec to $t = 18$ sec). At these different times, concomitant with the increase of convection and its development in the cavity, heat exchange takes place in the entire cavity too (see *Figure 7*). From $t = 10$ sec, nearly all the enclosure (80%) is subject to an obvious increase of temperature: the temperature varies from 600 K to 1500 K. This is observed even though the cavity is opened and the opening of the cavity seems to produce a distortion of the dynamic flow-field only, but not of the temperature field. The influence of the opening on the temperature field is first seen at $t = 25$ sec, when the cool air starts entering into the cavity and when the injection of hot gases is stopped. This is clearly shown in *Figure 5*, where a depression is created at the exit section. With buoyancy and convection, this fluid inflow stimulates the ventilation and cooling of the enclosure, and the velocity field is completely modified by the incoming flow, starting

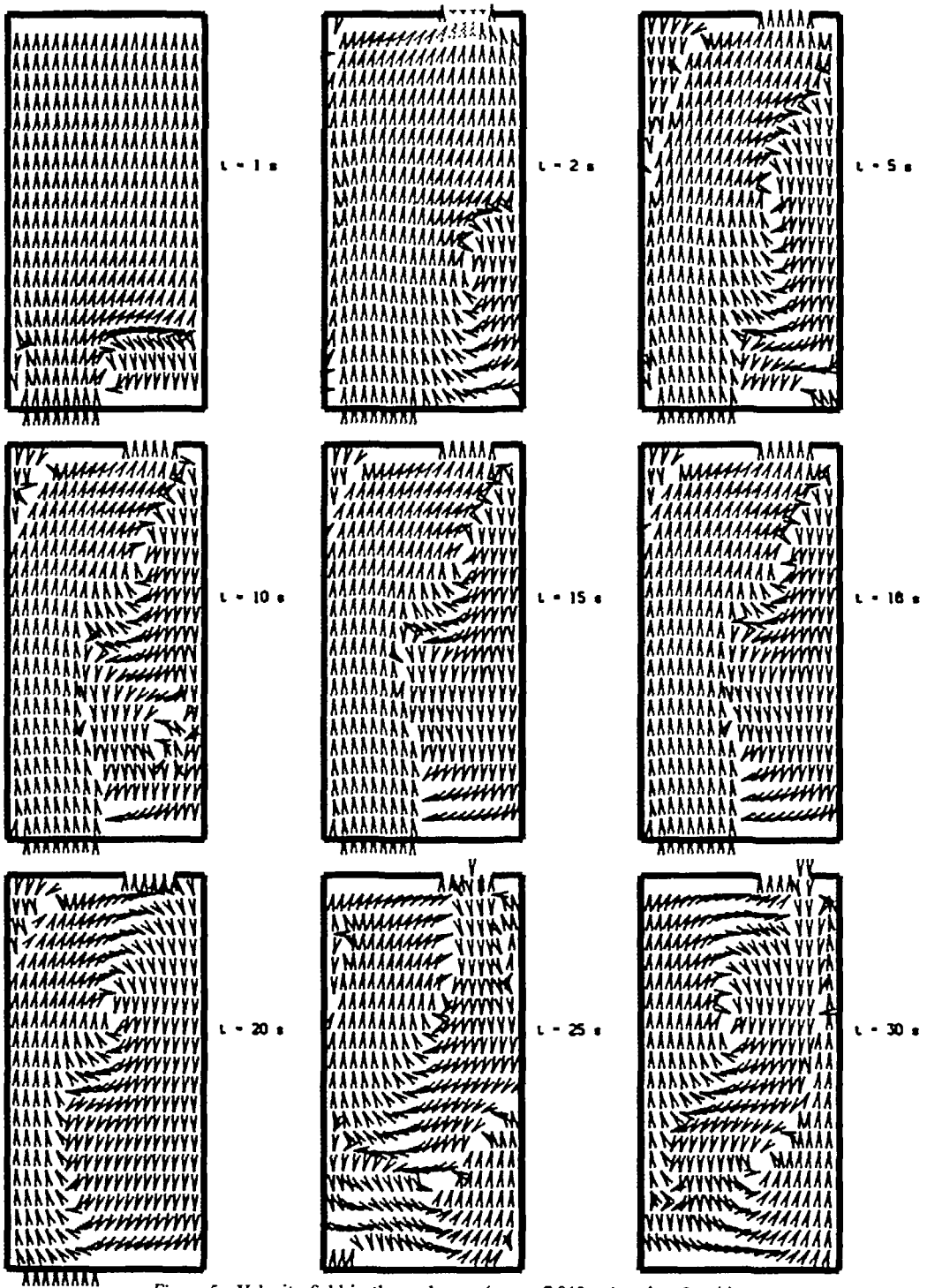

Figure 5 Velocity field in the enclosure (max = 7.019 m/s, min = 0 m/s)

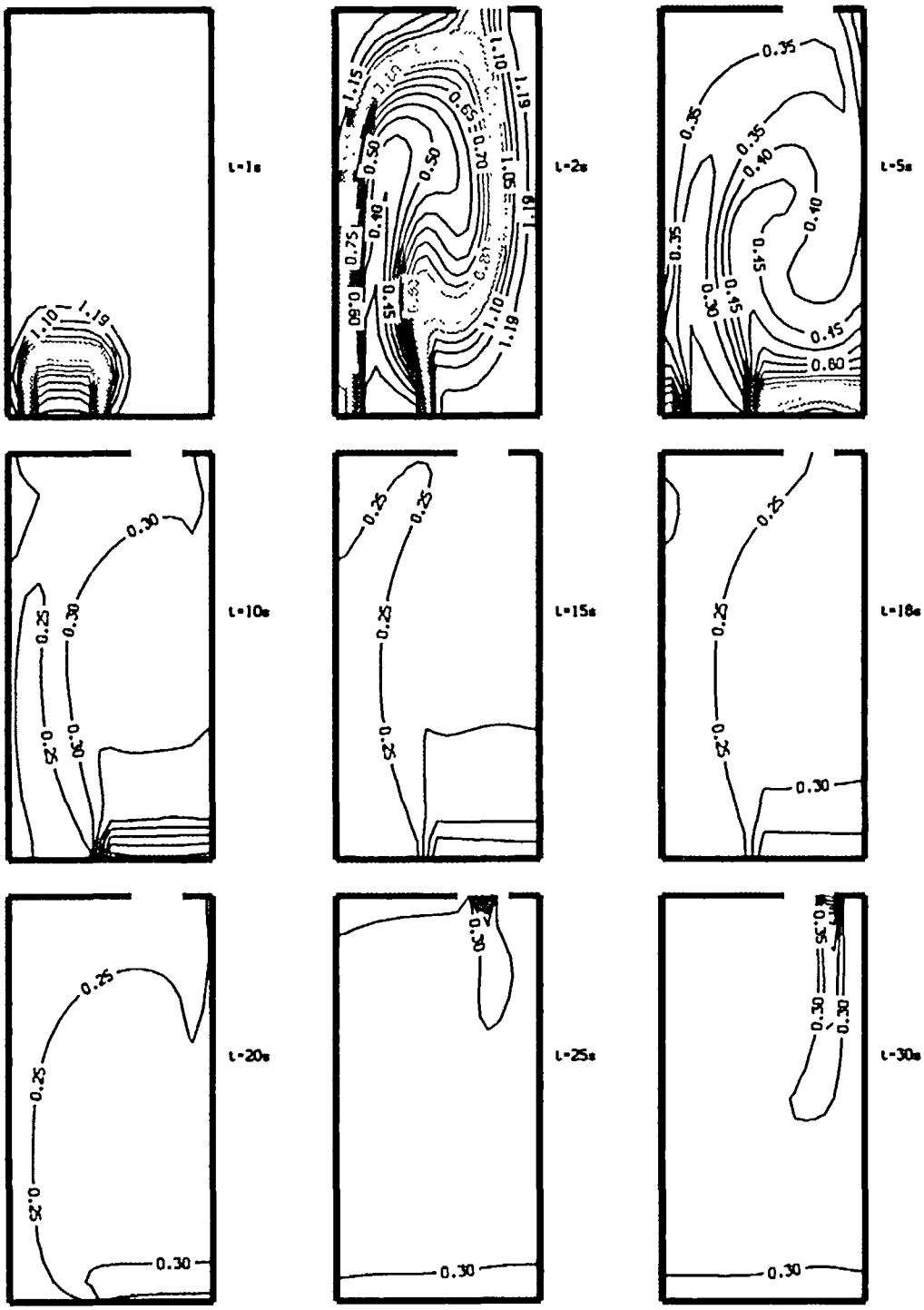

Figure 6 Density field in the enclosure (max = 1.2229 kg/m^3, min = 0.23 kg/m^3, incr = 0.05)

from $t = 25$ sec. In *Figure 6*, at the end of the injection period, an area of gas at uniform density equal to 0.30 kg/m^3 spreads on the bottom. At the same time, the incoming cool flow with density equal to 0.70 kg/m^3 (through the opening), expands rapidly due to the contact with hotter fluid: the density becomes equal to 0.30 kg/m^3 at $t = 30$ sec. These phenomena can be observed in *Figure 7*, where the cooling of the enclosure is obvious; the fall in temperature is

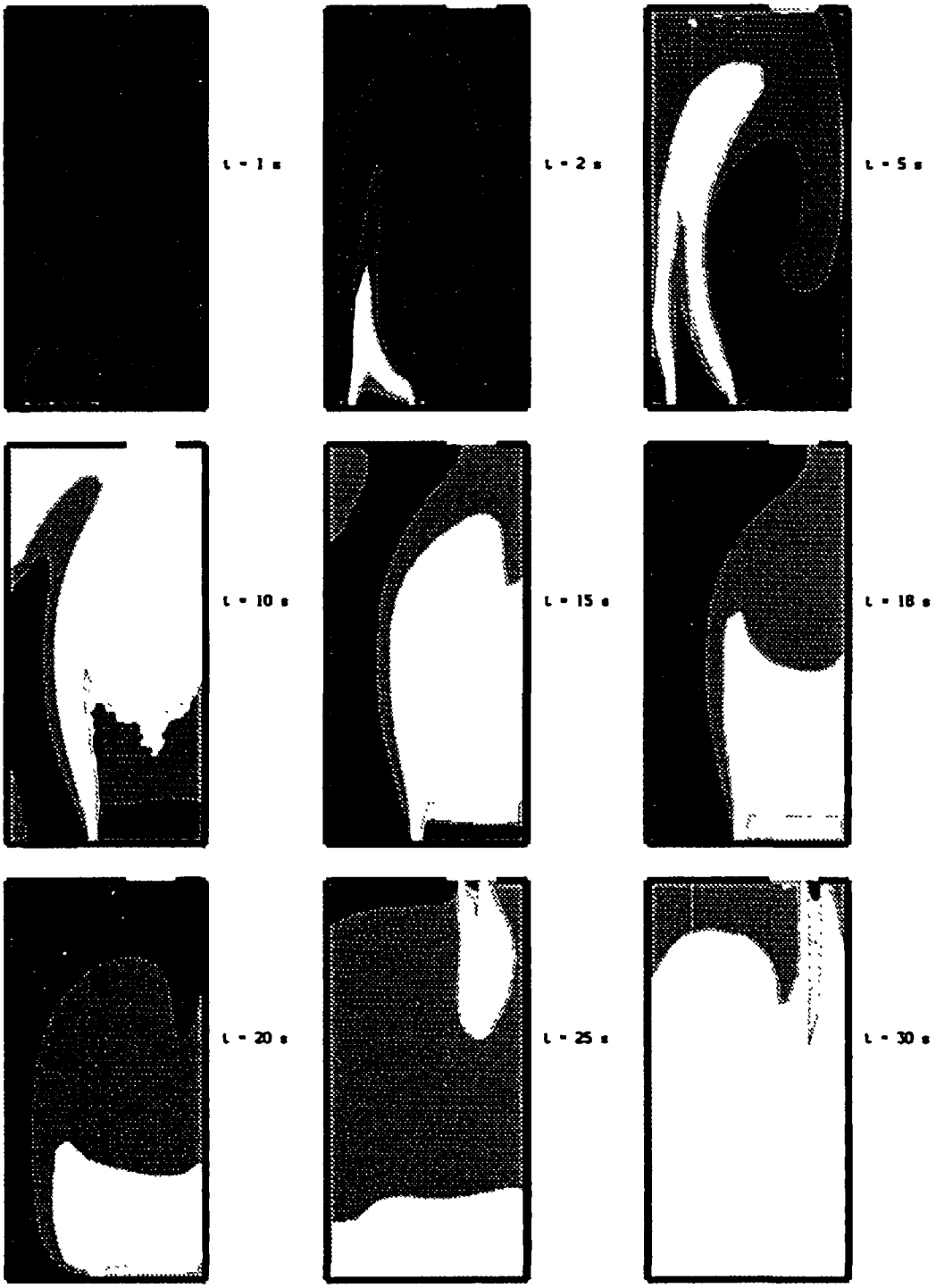

Figure 7 Temperature field in the enclosure (max = 1500 K, min = 300 K, incr = 50)

about 500 K–700 K, even though the cool flow is rapidly heated by conduction by the fluid in contact with it.

Radiative heat transfer

In this section, we study the effects of radiation on the flow pattern, by examining the same conditions while neglecting radiative heat transfer. *Figure 8* illustrates the temperature and

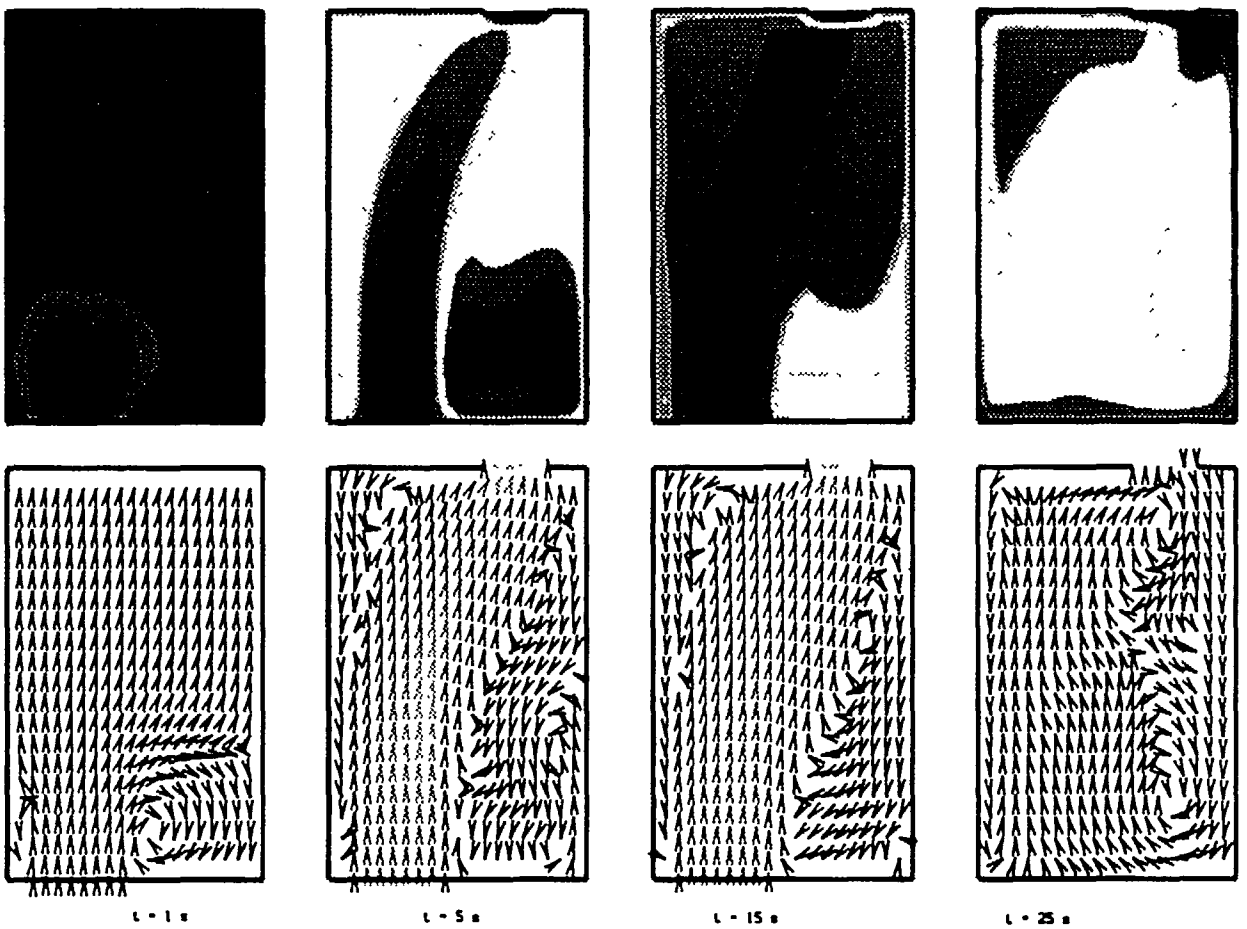

Figure 8 Temperature and velocity fields in the enclosure including radiant heat transfer (max = 1500 K, min = 300 K, incr = 50; max = 9.9 m/s, min = 0 m/s)

velocity fields only at four times, because of space limitations: $t = 1$ sec, $t = 5$ sec, $t = 15$ sec, $t = 25$ sec. These times selected are determined as far as possible to allow the best comparison with the case without radiative heat transfer.

At $t = 1$ sec, the results obtained in the two cases (with and without radiation) are very similar, because the walls temperatures reached are not high enough to make the parietal radiative heat transfer influence significant. At $t = 5$ sec, the velocity fields are still very similar to those obtained for the case neglecting radiation, because the flow pattern is essentially driven by the injection of mass at the bottom of the enclosure and by the vent of the cavity. Conversely, the analysis of the temperature field shows the important influence of the radiative heat transfer on the development of the isotherms. Taking into account these radiative effects, and couple the different heat transfers produces an increase of the temperature of the fluid near the walls the enclosure. Hence, the walls temperatures change rapidly owing to radiation and the temperature of the air is increasing by nearly pure conduction, as it is clearly shown in *Figure 8*, at $t = 15$ sec. At the opening section, the temperature of the fluid is about 300 K, because of the hypothesis related to the exit section: the vent is considered as a fictitious black surface whose the temperature is equal to the temperature of the fluid contained in the infinite tank[26]. When the injection of hot gases is stopped (from $t = 20$ sec), we can note a specific flow field: an incoming cool flow at $T = 300$ K appears at the vent and moves downward along the right side of the enclosure, unlike the case neglecting the radiative heat transfer. The influence of convection on the

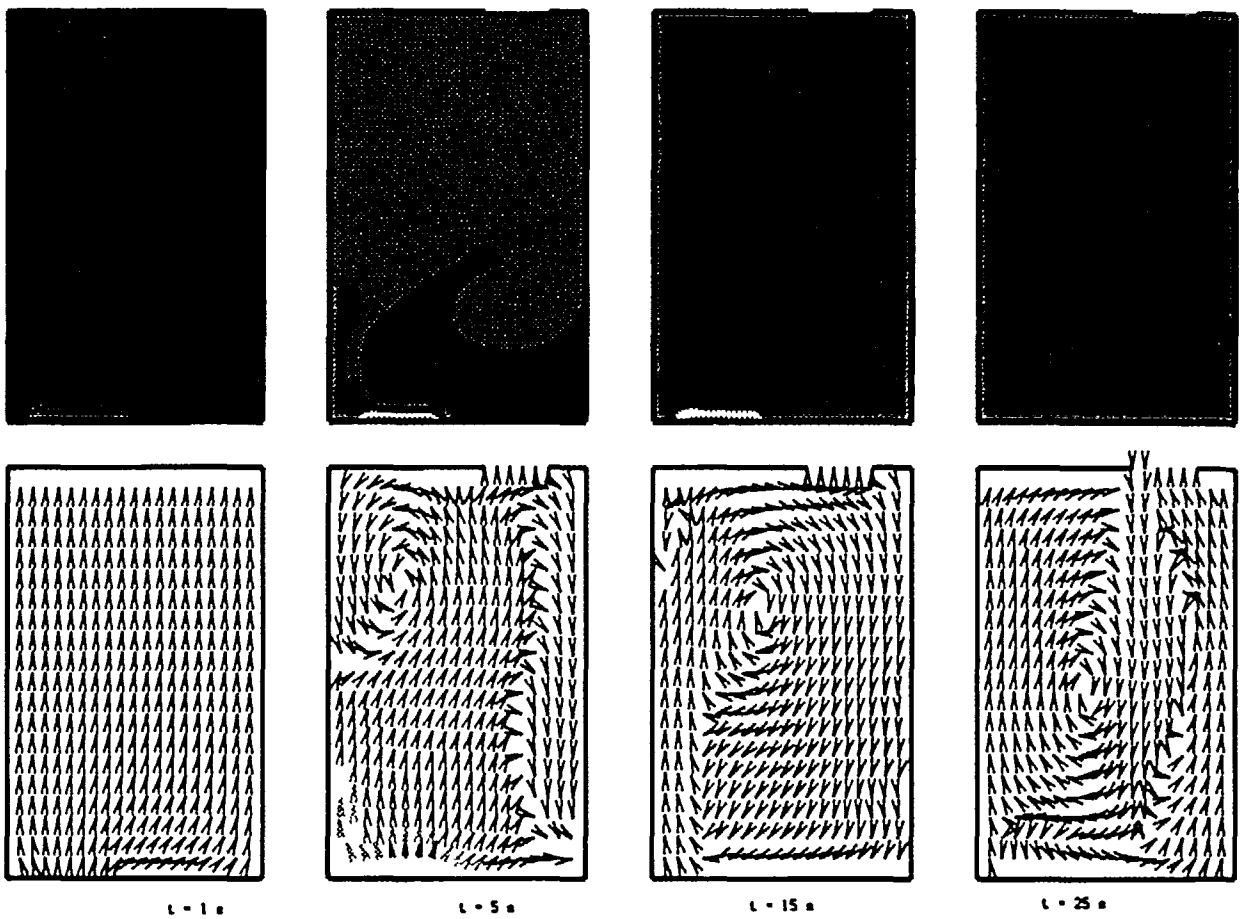

Figure 9 Temperature and velocity fields in the enclosure with natural convection (max = 1500 K, min = 300 K, incr = 50; max = 5.58 m/s, min = 0 m/s)

temperature profiles is obvious and the temperature field becomes completely different from those obtained in the previous case, which consists of superposed isotherms. Therefore, it follows from the comparison between the results obtained with and without radiation, that the development of the velocity field without radiation is very different from those including radiative heat transfer, the major difference being that no clockwise eddy appears at the center of the enclosure in the second case. The isotherms are also considerably modified.

Natural convection

The effects of the injection of hot gases on the thermal heat transfer and the velocity field are studied, in this section, by examining the specific case of a mass flow rate equal to zero. The injection area is the same as the case of forced convection and is supposed to be heated at a uniform temperature equal to 1500 K until $t_3 = 20$ sec. In this simulation only the temperature gradient, and so the density gradient, produce fluid motion. It is clearly obvious that the temperature and velocity are very different to those of the forced convection, as shown in *Figure 9*. The development of the isotherms is very slow and the convective currents are small. So the entire enclosure is slowly subject to a small increase of temperature up to $t = 5$ sec, only the hot surface area takes part in heat transfer. Almost the whole cavity is at about 400 K at $t = 5$ sec. However, the overpressure is reached at $t = 3$ sec (see *Figure 11*), and hot gases escape through

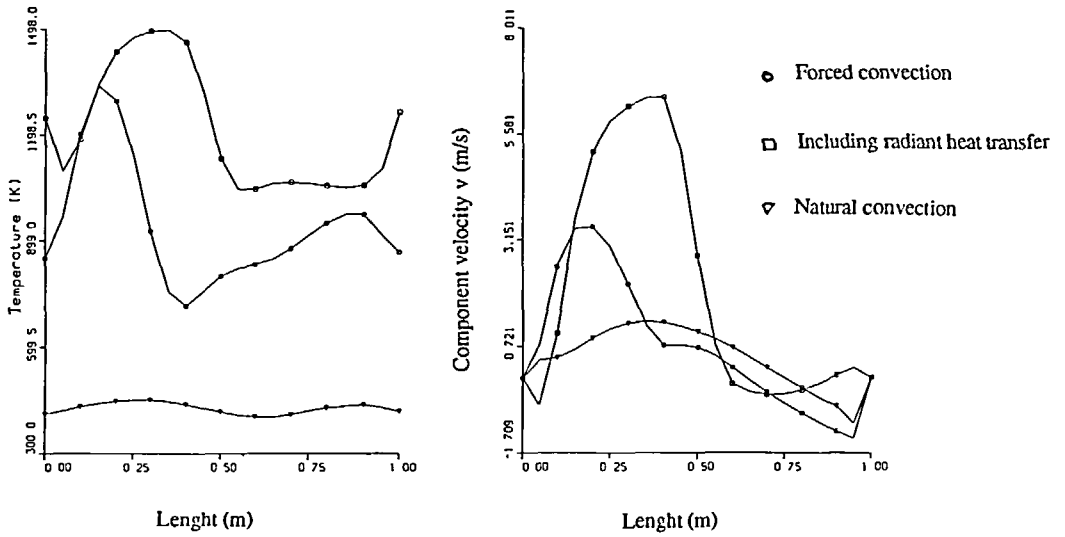

Figure 10 Temperature and velocity profiles at enclosure mid-height at t = 5 s

the vent to the exterior. Gases in contact with hot wall are heated by conduction, and become light. A swift upward current also appears on the hot surface and the enclosed fluid is swept along the current. From $t = 25$ sec, incoming cool flow appears at the exit section. Due to the gradient of density, it moves downward relatively rapidly and mixes with the enclosed hot fluid.

Comparison forced convection/radiative heat transfer/natural convection

Figure 10 illustrates the velocity and temperature profiles at mid-height at $t = 5$ sec to compare heat transfer and dynamics field for the preceding three cases studied and entitled forced convection, forced convection including radiative heat transfer and natural convection. The influence of radiation is very large as indicated in *Figure 10*. When the injection of hot gases is considered, it constitutes the main factor to the fluid motion. The profile of the component of the velocity v is clearly influenced by this action. The component v of the velocity reaches a maximum when the radiative heat transfer is included. The maximal value is equal to 6.36 m/s. It is located up on the injection area due to the injection of hot gases, and to the recirculated air near the injection points. This maximum is nearly double the value obtained when radiation is neglected. Therefore, the radiative heat transfer induces much stronger convective currents, and near the walls, these profiles are in fact opposite to those induced by convection alone (forced convection and natural convection). The difference of the maximal value of v between forced convection and natural convection is about 60%. In all cases, we can note negative profile of v from $l = 0.5$ m induced by the cool fluid which moves downward along the right side of the enclosure. As a result the temperature distribution in the enclosure is considerably altered as shown in *Figure 10*. When radiation is considered, the walls temperature is greater than that of the fluid, except at the local hot spot centred on the area above the injection points. In this case, the fluid temperature is greater than those obtained in the other cases. The temperature profile for natural convection is very homogeneous and about 400 K. When only injection of hot gases is studied, the temperature distribution is very irregular, with a maximal value equal to 1300 K due to the heat and mass source and to the effects of the fluid compressibility. The fall of the temperature after the injection points is produced by the cool fluid currents, as shown in *Figure 7*.

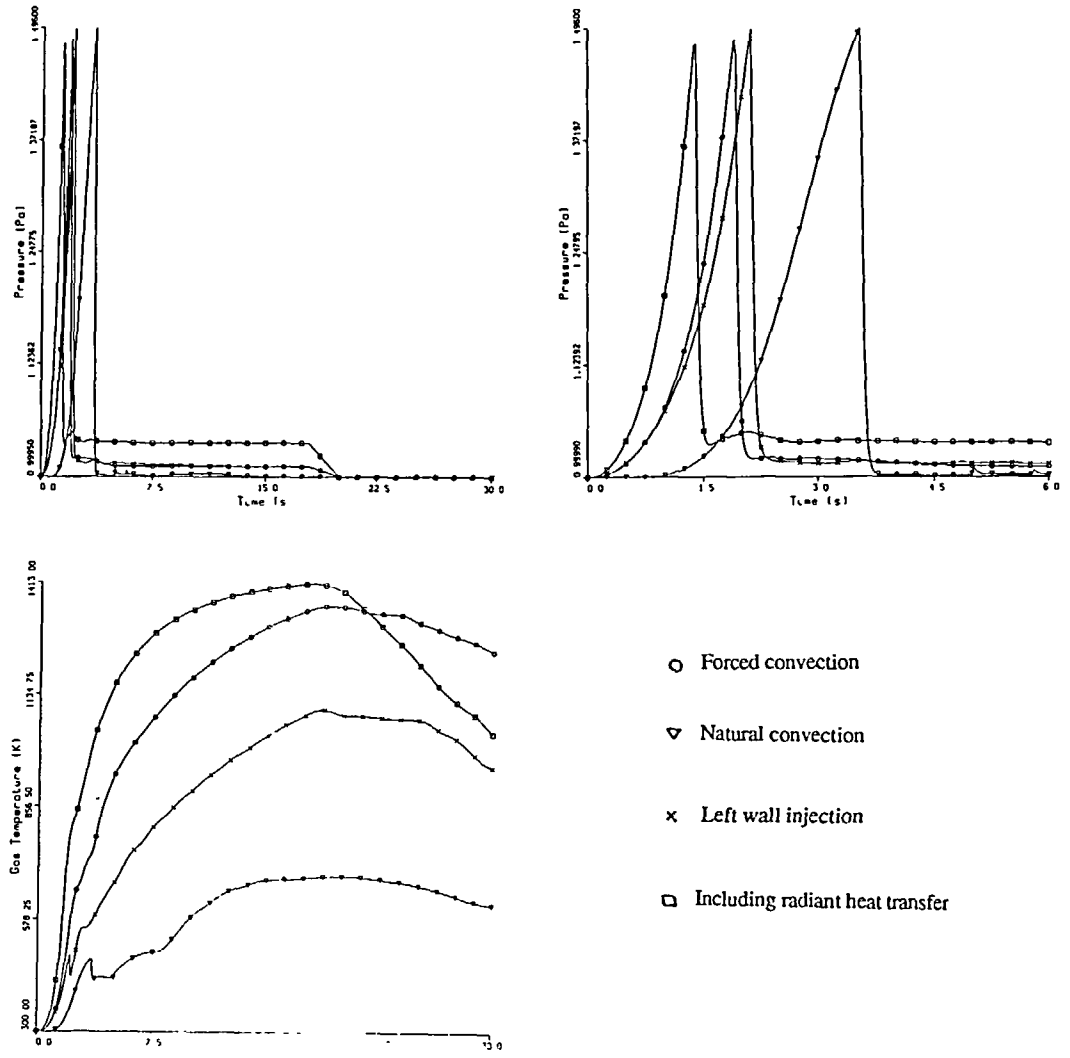

Figure 11 Average temperature and average pressure evolutions in the enclosure

The comparison between the average temperatures and the average pressures in the different cases give predictable results. The analysis of the evolution of the average temperatures shows an increase of temperature in all cases until the end of the hot gases injection, or until the end of the heating of the surface ($t = 18$ sec). The opening of the enclosure about 2 sec or about $t = 3$ sec in the natural convection case, does not lead to a decrease in the average temperature, except for natural convection. The heat losses are smaller than the heat given by the hot source. These results show the role of the radiative heat transfer in an enclosure when high temperatures are used. The maximal average temperature is equal to 1413 K at $t = 18$ sec. The injection of mass in a closed or partially open cavity also plays a key role, and the maximal value in forced convection is about double those obtained in natural convection (respectively about 1200 K and 600 K). Even when incoming cool flow appears at the vent of the enclosures, it is worthy of

note that taking into account radiation is really important in the evolution of heat transfer: we can see the rapid fall of the average temperature produced by the incoming flow in contact with the right sidewall of the cavity.

The study of average pressures leads to a brief remark, because the results are very similar whatever the kind of convection is studied: the increase of the temperature corresponds to an increase of average pressure, until the enclosure opens to the exterior when the overpressure is reached. Then we can see the pressure falls to the initial value, the major difference being that the overpressure is reached at various times.

Parametric study

Effects of the injection location

The effect of the location of the injection points on the heat transfers are examined first in this second section, with the same conditions as for the general study. *Figure 12* represents the isotherms and velocity fields at four specific times. Radiative heat transfer are not taken into account in this study.

At $t = 1$ sec, we can note the vertical development of the temperature isolines to the top of the enclosure and, while the cavity is closed, the flow pattern consists of a only one clockwise eddy. When the overpressure is reached, the cavity opens to the exterior and the convective

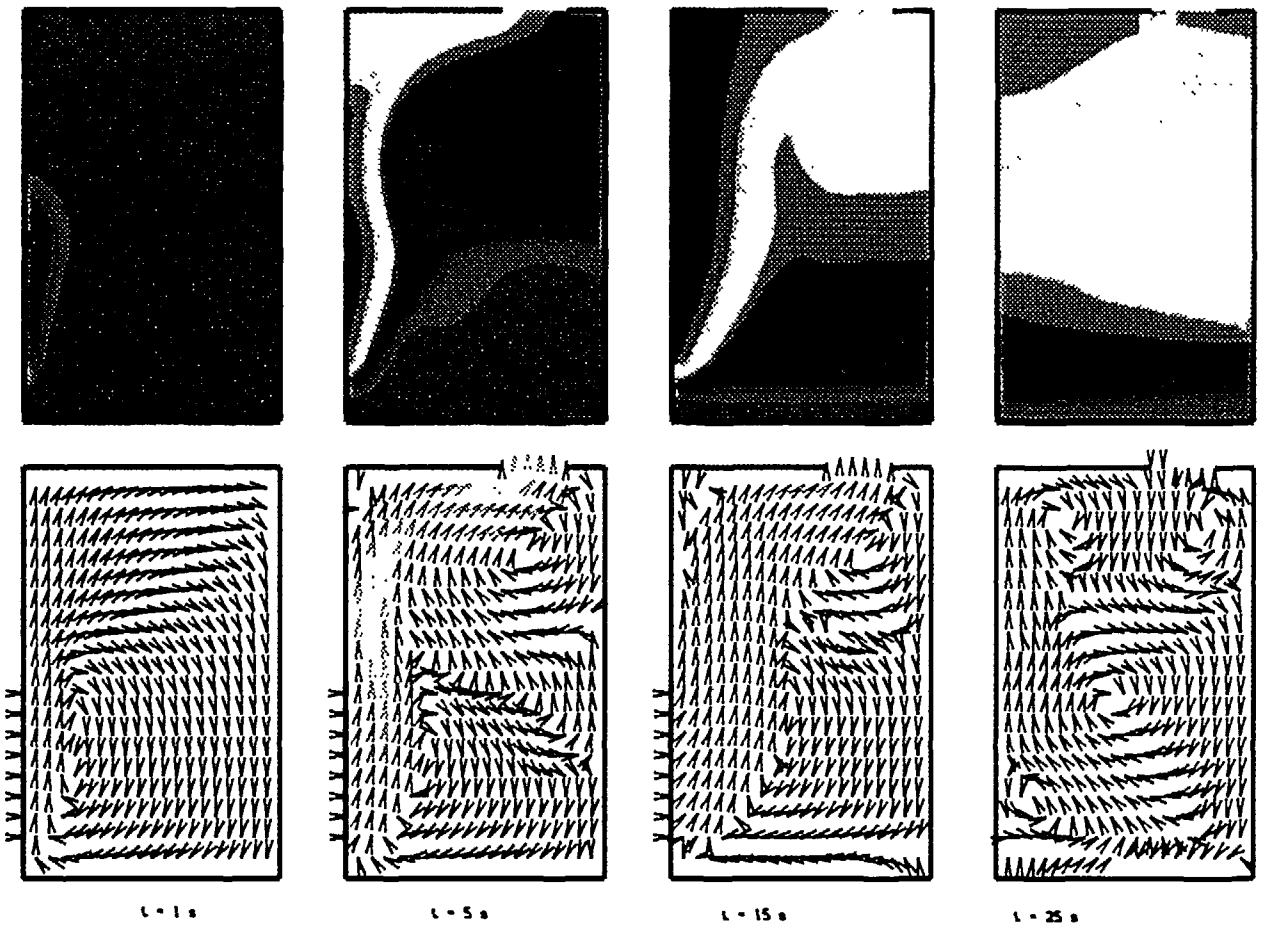

Figure 12 Temperature and velocity fields in the enclosure for a left wall injection neglecting radiant heat transfer (max = 1500 K, min = 300 K, incr = 50; max = 4.66 m/s, min = 0 m/s)

motion strongly influences the development of the isotherms. Heat transfers are located only at the top of the enclosure. The result is the opposite to that obtained for the bottom injection of hot gases, where we noted a great homogenization of heat transfer. The horizontal development of the isotherms increases as time progresses. At $t = 25$ sec, the superposition of isothermal layers is obvious. At this moment, the incoming cool flow is lower than for the case of the injection located on the floor because the cool flow is rapidly swept along by two eddies, with opposite directions, near the opening. It is rapidly mixed with hot gases and cannot circulate in the entire enclosure. With regard to the velocity field, the results show a more complex development of the convective currents constituted by several eddies, which cannot allow a significant development of heat transfer. These differences in the flow pattern lead to obvious differences in the evolution of the average temperature of the fluid with respect to the first case studied (see *Figure 11*). The maximal value of the temperature is less greater than those of the bottom injection (respectively 1098 K and 1355 K). The two-dimensional treatment of this problem is currently straightforward because of the differences in the average temperature distributions.

Influence of the opening ratio A_0

This section deals with the influence of the opening ratio A_0 ($A_0 = 1/5$, 2/5, 3/5, 1) of the enclosure on the heat transfer and velocity field. To simplify the parametric study, we have

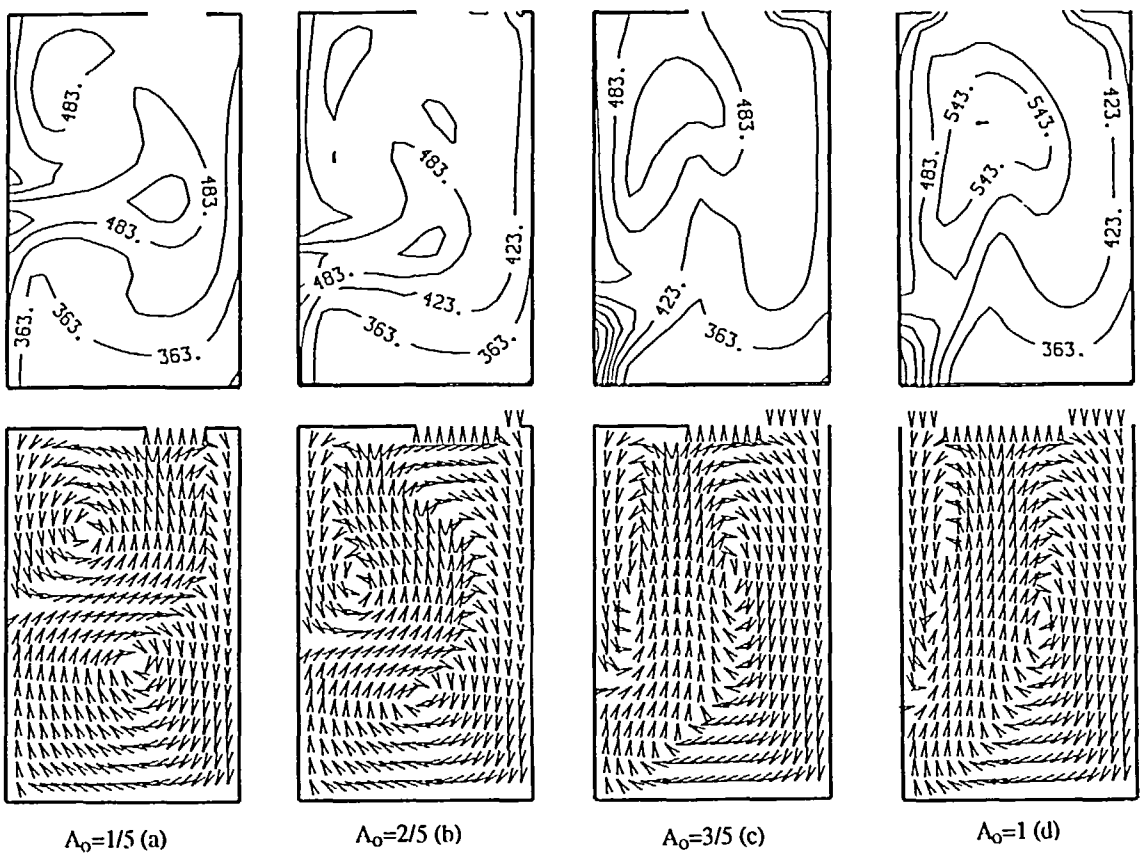

Figure 13 Temperature and velocity distributions at t=3 s for A_0=1/5 (a), A_0=2/5 (b), A_0=3/5 (c), A_0=1 (d)

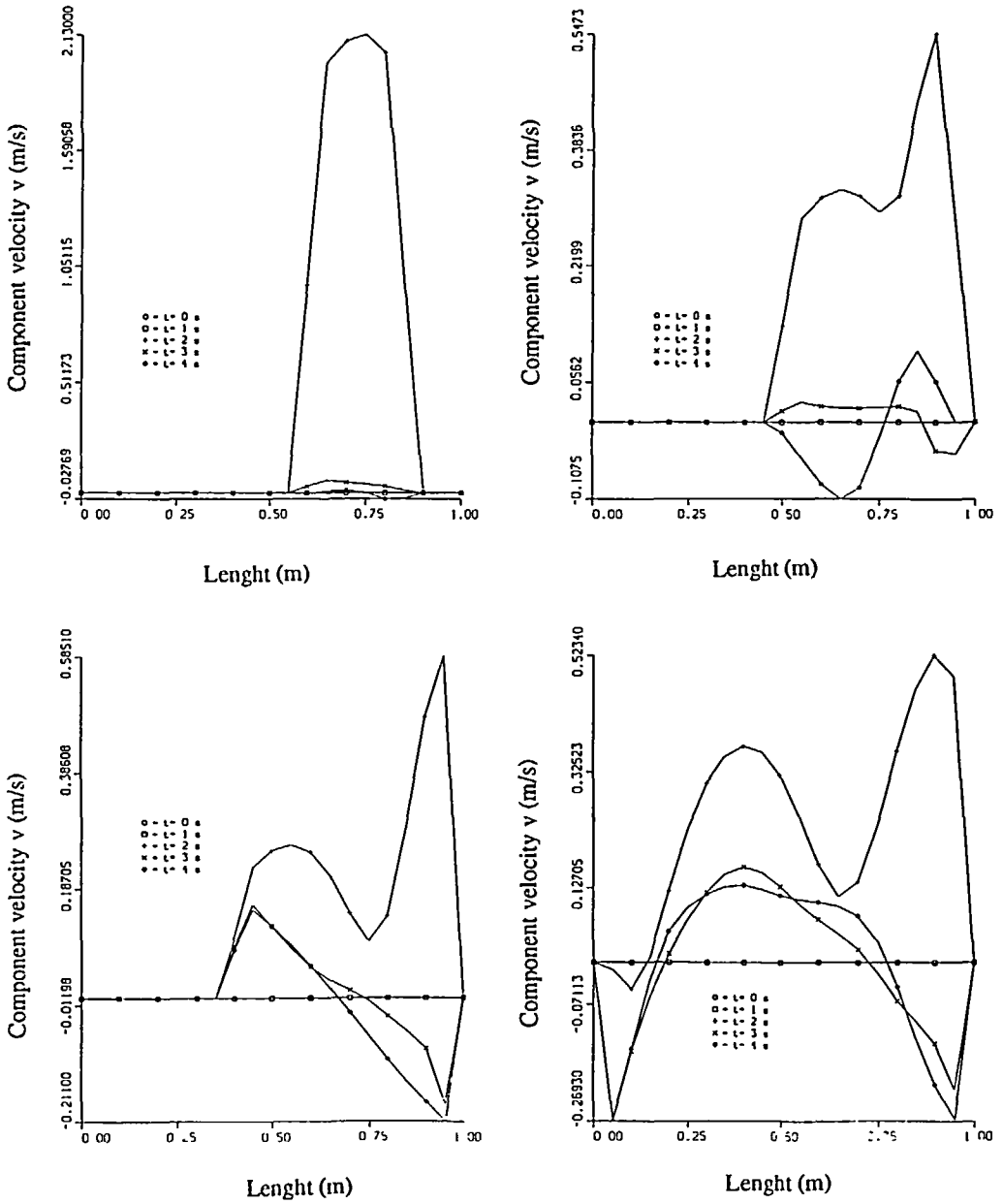

Figure 14 Velocity profiles at opening for different A_0 values

considered a constant mass flow rate equal to 0.01 kg/sec. The hot gases are injected for 2 sec at a uniform temperature equal to 1500 K. An overpressure about 500 mbar is reached at $t = 1.9$ sec. The phenomena are studied until $t = 4$ sec, so that the incoming cool flow can be observed simultaneously with the outcoming hot gases through the vent.

Figure 13 represents the temperature and velocity profiles in the enclosure at $t = 3$ sec for the four values of the opening ratio. The evolutions of temperature and velocity at $t = 1$ sec and at

$t = 2$ sec are not presented here: the results are very similar for all the values of the opening ratio, because the overpressure, which produces the opening of the enclosure, is reached at $t = 1.9$ sec. The area of injection is the same for the test cases, and we can note that increasing the opening ratio A_0 produces an increasing of hot gas recirculation due to the downward movement of cool gases along side walls. For $A_0 = 1/5$ and $A_0 = 2/5$, the flow pattern is disturbed because it is made up of two clockwise eddies. It seems to be more structured for the other values of the opening ratio: the main flow is almost vertical, because the outcoming and the incoming flows are greater. For $A_0 = 1$, the incoming cool moves downward along the two side walls. At $t = 3$ sec, we can see that there is only an outcoming flow for $A_0 = 1/5$ while for the other values of A_0 there are simultaneously an outgoing and incoming flows. These results are confirmed by the results presented in *Figure 14*, which shows the distributions of the component of the velocity v at the different times at the vent section. For $A_0 = 1/5$, at $t = 2$ sec, the profile of v is those specific to an exit section, with a maximal value equal to 2.13 m/sec. At the same time, for the other opening ratio, the velocity distributions are very different; they seem to be discontinuous profiles, with maximal values equal to 0.54 m/sec, 0.58 m/sec and 0.52 m/sec. From $t = 3$ sec, velocity profiles change sign as a function of x, with a maximum about 2.67 m/sec ($A_0 = 1$). In this case, a symmetric profile of the v component seems to appear due to the geometric aspect of the enclosure.

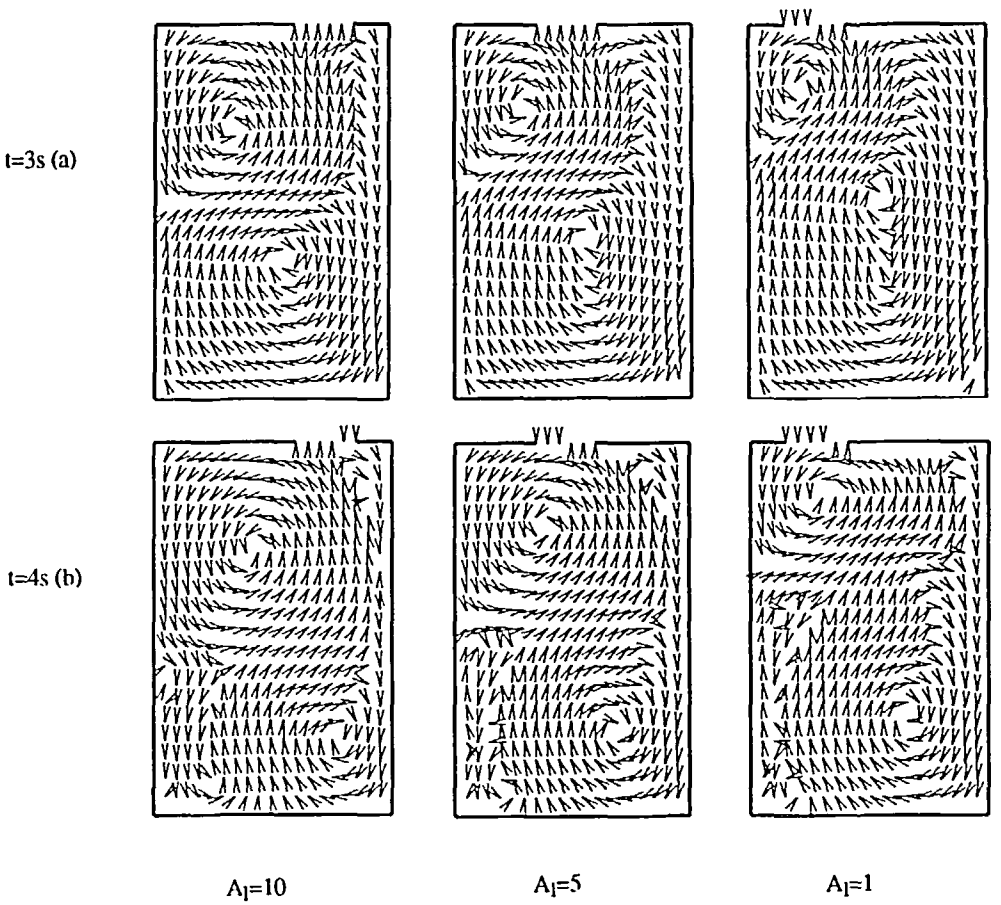

Figure 15 Temperature and velocity distributions at t=3 s (a) and at t=4 s (b) for different A_1 values: $A_1 = 10$, $A_1 = 5$, $A_1 = 1$

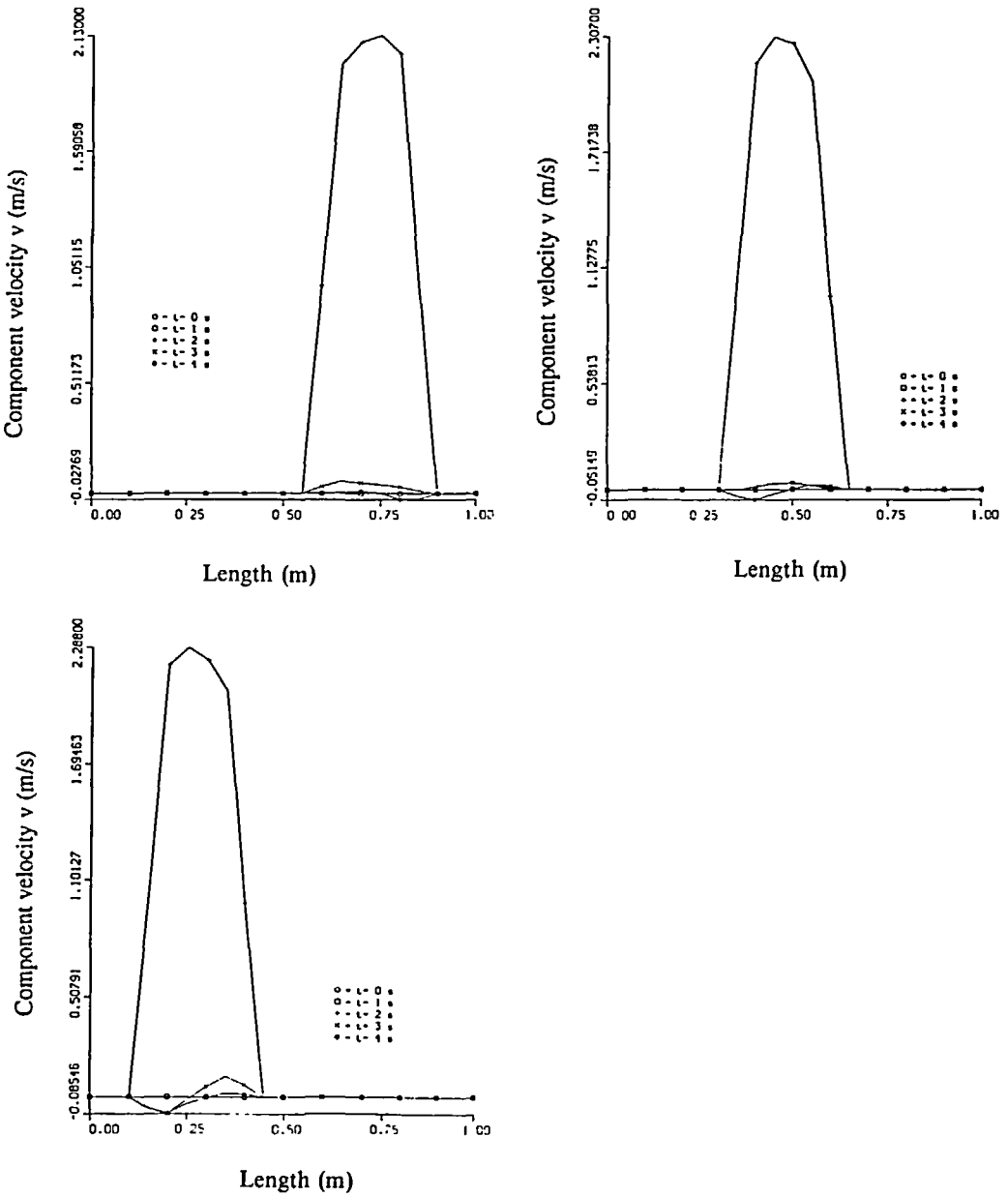

Figure 16 Velocity profiles at opening for different A_1 values

Influence of the location ratio A_l

In this part, the effect of the location ratio A_l on the flow structure is analyzed. Three values of A_l are studied: $A_l = 10, 5, 1$. The opening ratio is here equal to 1/5, and the mass flow rate equal to 0.01 kg/sec. The results (*Figure 15*) presented correspond to $t = 3$ sec and $t = 4$ sec. Because of space limitations and their little interest, the results at $t = 1$ sec and $t = 2$ sec are not presented here: there is not a great distance between these test cases, except for the distortion

of the main flow produced directly by the injection of hot gases and by the vent. When the injection is stopped (at $t = 3$ sec) we can observe a flow divided into two parts: the partition is more important when the location ratio is great.

An anti-clockwise eddy appears in the superior half of the enclosure, which holds about 1/3 ($A_l = 1$) of the height of the cavity as long as it holds the half of the enclosure when $A_l = 10$. At $t = 4$ sec, we can see for all cases presented that the flow is separated in two eddies: one in the inferior half of the enclosure and the second in the superior part. The limit between these two flows varies as a function of the location ratio A_l. By increasing the value of A_l, the eddy located in the superior part grows. These differences in the flow pattern, induced by the location ratio, do not produce a great effect about the velocity profiles at the exit section (see *Figure 16*). A positive and negative profile is first seen at $t = 3$ sec in the case of $A_l = 1$, like it is shown in *Figure 15*. The maximal value is almost insensitive to the variations in the location of the vent with respect to the injection points, and is about 2.2 m/s. This value is obtained when the overpressure is reached and when the cavity opens to the exterior.

CONCLUDING REMARKS

In this paper, a modified ICE method for computing 2D compressible unsteady flows in cavities has been presented. One of the interests of this study is the numerical treatment of a low-Mach number flow induced by an injection of hot gases into a cavity. Moreover, outgoing flow from the enclosure, as well as the later development of an incoming cool flow into the cavity, from the exterior, at the exit section, have justified the treatment of the opening of the enclosure by resolution of a Riemann problem. Indeed, such a treatment is the more convenient to deal with all of possible flow patterns. The results show the effects of the location of the hot gas injection, the influence of the vent upon the flow patterns. These indicate that the radiation dominates the heat transfer and significantly alters the convective motions.

The compressibility of the fluid has been taken into account, contrary to numerous studies about convection in enclosures, where the Boussinesq approximation is usually made, and the injection of hot gases is found to play a key role on the temperature and velocity distributions in the enclosure.

ACKNOWLEDGEMENTS

This work was supported by DCN/GERPy Toulon France.

APPENDIX

Difference equation of momentum

The momentum equation is differenced in terms of fluxes: these terms consist of two components: a spatially centred term and a donor cell (or upwind) term. The donor cell parameter α, $0 \leqslant \alpha \leqslant 1$, determines the fraction of each component in the total mass flux.

For the momentum equations, the convection terms are not written in terms of momentum fluxes, but as edge-centered fluxes of a velocity gradient.

For the x-momentum equation, the convection terms are:

$$FUX = \left(u\frac{\partial u}{\partial x}\right)^n_{i+1/2,j} = \frac{(1-\alpha)}{2\delta x} u^n_{i+1/2,j}(u^n_{i+3/2,j} - u^n_{i-1/2,j})$$
$$+ \frac{\alpha}{2\delta x}[(u^n_{i+3/2,j} - u^n_{i+1/2,j})(u^n_{i+1/2,j} - |u^n_{i+1/2,j}|)$$
$$+ (u^n_{i+1/2,j} - u^n_{i-1/2,j})(u^n_{i+1/2,j} + |u^n_{i+1/2,j}|)]$$
$$FUY = \left(v\frac{\partial u}{\partial y}\right)^n_{i+1/2,j} = \frac{(1-\alpha)}{2\delta y} v^n_{i+1/2,j}(u^n_{i+1/2,j+1} - u^n_{i-1/2,j-1})$$
$$+ \frac{\alpha}{2\delta y}[(u^n_{i+1/2,j+1} - u^n_{i+1/2,j})(v^n_{i+1/2,j} - |v^n_{i+1/2,j}|)$$
$$+ (u^n_{i+1/2,j} - u^n_{i+1/2,j-1})(v^n_{i+1/2,j} + |v^n_{i+1/2,j}|)]$$

where

$$v^n_{i+1/2,j} = 0.25[v^n_{i+1,j+1/2} + v^n_{i+1,j-1/2} + v^n_{i,j+1/2} + v^n_{i,j-1/2}]$$

The complete x-momentum difference equation is:

$$\frac{u_{i+1/2,j} - u^n_{i+1/2,j}}{\delta t} + FUX + FUY = g_x - \frac{2}{\delta x}\frac{\bar{P}_{i+1,j} - \bar{P}_{i,j}}{\rho^n_{i+1,j} + \rho^n_{i,j}}$$
$$+ \frac{2\mu}{(\rho^n_{i+1,j} + \rho^n_{i,j})}\left\{\frac{4}{3\delta x^2}[u^n_{i+3/2,j} - 2u^n_{i+1/2,j} + u^n_{i-1/2,j}]\right.$$
$$+ \frac{1}{\delta y^2}[u^n_{i+1/2,j+1} - 2u^n_{i+1/2,j} + u^n_{i+1/2,j-1}]$$
$$\left.+ \frac{1}{3\delta x\delta y}[v^n_{i+1,j+1/2} - v^n_{i+1,j-1/2} - v^n_{i,j+1/2} + v^n_{i,j-1/2}]\right\}$$

where $\bar{P}$ is an estimate of the advanced time pressure.

REFERENCES

1 Torrance, K. E., Orloff, L. and Rockett, J. A. Experiments on natural convection in enclosures with localized heating from below, *J. of Fluid Mechanics*, **36**, 1, 21–31 (1969)
2 Torrance, K. E. and Rockett, J. A. Numerical study of natural convection in an enclosure with localized heating from below, *J. of Fluid Mechanics*, **36**, 1, 33–54 (1969)
3 Greenspan, D. and Schultz, D. Natural convection in an enclosure with localized heating from below, *Comp. Meth. in Applied Mech. and Eng.*, **3**, 1–10 (1974)
4 May, H. O. A numerical study on natural convection in an inclined square enclosure containing internal heat sources, *Int. J. of Heat and Mass Transfer*, **34**, 919–928 (1991)
5 Allançon, L., Porterie, B., Loraud, J. C. and Daniel, E. Unsteady convection in a cavity due to pyrolysis, *Mechanics Research Communications*, **20** (2), 173–179 (1993)
6 Larson, D. W. and Viskanta, R. Transient combined laminar free convection and radiation in a rectangular enclosure, *J. of Fluid Mechanics*, **78**, 1, 65–85 (1976)
7 Allançon, L., Porterie, B. and Loraud, J. C. Etude des transferts radiatifs et convectifs induits par une source de chaleur et de masse dans une cavité à deux zones, to appear in *Int. J. of Heat and Mass Transfer*
8 Penot, F. Numerical calculation of two-dimensional natural convection in isothermal open cavities, *Num. Heat Transfer*, **5**, 421–437 (1982)
9 Le Quere, P., Humphrey, J. A. C. and Sherman, F. S. Numerical calculation of thermally driven two-dimensional unsteady laminar flow in cavities of rectangular cross section, *Num. Heat Transfer*, **4**, 249–283 (1981)

10 Chan, Y. L. and Tien, C. L. A numerical study of two-dimensional natural convection in square open cavities, *Num. Heat Transfer*, **8**, 65–80 (1985)
11 Miyamoto, M., Kuen, T. H., Goldstein, R. J. and Katoh, Y. Two-dimensional laminar natural convection heat transfer from a fully or partially open square cavity, *Num. Heat Transfer, A*, **15**, 411–430 (1989)
12 Humphrey, J. A. C. and To, W. M. Numerical simulation of buoyant turbulent flow—free and mixed convection in a heated cavity, *Int. J. of Heat and Mass Transfer*, **29**, 4, 593–610 (1986)
13 Humphrey, J. A. C., Miller, L. and Chen, K. S. Experimental investigation of thermally driven flow in open cavities of rectangular cross-section, *Mechanical Engineering Rept. FM-81-2*, Univ. of California, Berkeley (1981)
14 Sernas, V. and Kyriakides, L. Natural convection in an open cavity, *Heat Transfer 1982: Proc. of the Seventh Int. Heat Transfer Conf.*, **2**, Hemisphere, Washington, D.C., NC26, 275–280 (1982)
15 Hess, C. F. and Henze, R. H. Experimental investigation of natural convection losses from open cavities, *J. Heat Transfer*, **106**, 333–338 (1984)
16 Chen, K. S., Humphrey, J. A. C. and Sherman, F. S. Free and mixed convection flow of air in a heated cavity of variable rectangular cross section and orientation, *Phil. Trans. Roy. Soc. Lond.*, **A316**, 57–84 (1985)
17 Chan, Y. L. and Tien, C. L. Laminar natural convection in shallow open cavities, *Trans. ASME, J. Heat Transfer*, **108**, 305–309 (1986)
18 Doria, M. L. A numerical model for the prediction of two-dimensional unsteady flows of multicomponent gases with strong buoyancy effects and recirculation, *Notre Dame Rept. TR-37191-74-4* (1974)
19 Sefcik, D. M., Webb, B. W. and Heaton, H. S. Analysis of natural convection in vertically-vented enclosures, *Int. J. of Heat and Mass Transfer*, **34**, 12, 3037–3046 (1991)
20 Yang, K. T. Transitions and bifurcations in laminar buoyant flows in confined enclosures, *J. of Heat Transfer*, **110**, 1191–1204 (1988)
21 Ostrach, S. Natural convection in enclosures, *J. of Heat Transfer*, **110**, 1175–1190 (1988)
22 Gray, D. D. and Giorgini, A. The validity of the Boussinesq approximation for liquids and gases, *Int. J. of Heat and Mass Transfer*, **19**, 545–551 (1976)
23 Fernandez, G. and Guillard, H. A numerical method for the computation of low Mach number reactive flows, *Num. Meth. in Lam. and Turb. Flow*, **6**, 1, 815–825 (1989)
24 Harlow, F. H. and Amsden, A. A. A numerical fluid dynamics calculation method for all flow speeds, *J. of Comp. Physics*, **8**, 197–213 (1971)
25 Sparrow, E. M. and Cess, R. D. *Radiation Heat Transfer*, Belmont, California: Brooks/Cole Publishing (1966)
26 Toor, J. S. and Viskanta, R. A critical examination of the validity of simplified models for radiant heat transfer analysis, *Int. J. of Heat and Mass Transfer*, **15**, 1553–1567 (1972)
27 Beam, R. and Warming, R. F. An implicit factored scheme for the compressible Navier–Stokes equations, *AIAA Journal*, **16**, 4, 393–402 (1978)
28 MacCormack, R. W. The effect of viscosity in hypervelocity impact cratering, *AIAA Paper 69-354*, Cincinnati, Ohio (1969)
29 MacCormack, R. W. Current states of numerical solutions of the Navier–Stokes equations, *AIAA Paper 85-0032*, Reno, USA (1985)
30 Van Leer. Toward the ultimate conservative scheme V: second order sequel to Godunov scheme, *J. Comp. Phys.*, **32**, 101–133 (1979)
31 Chakravarthy, S. R. Euler equations—implicit schemes and boundary conditions, *AIAA J.*, **21**, 5 (1983)
32 Gottlieb, J. Lecture course notes on Random-choice method for solving one-dimensional unsteady flows in ducts, shock tubes and blast-wave simulators, presented at AC-Laboratorium Spiez, Switzerland (1986)